# An investigation of heat transfer augmentation and friction characteristics in solar air heater duct with V-shaped wire as artificial roughness on absorber plate

**Madhukeshwara N.[1], E. S. Prakash[2]**

[1] Department of Mechanical Engineering, B.I.E.T, Davanagere, Karnataka, India.
[2] Department of Studies in Mechanical Engineering, U.B.D.T.C.E, Davanagere, Karnataka, India.

**Abstract**
An experimental investigation of heat transfer augmentation and friction characteristics of fully developed turbulent flow in a rectangular duct of solar air heater with absorber plate having V-shaped wire ribs as artificial roughness on its underside is carried out. The investigation covers wide range of different parameters of wire ribbed roughness: relative roughness pitch (p/e) from 10 to 40, relative roughness height (e/$D_h$) from 0.01 to 0.04 and angle of attack of flow ($\alpha$) from 20° to 90°. Duct aspect ratio (W/B) is kept 5 and Reynolds number (Re) is varied from 2,500 to 8,500. The heat transfer and friction factor values obtained are compared with those of smooth duct under similar flow conditions. Expressions are developed for Nusselt number and friction factor for the roughness geometry. Enhancement of Nusselt number and friction factor for roughened duct are 1.5 and 2.7 times of smooth duct respectively.

**Keywords:** Heat transfer; Friction factor; Wire ribbed absorber; Nusselt number.

## 1. Introduction
Solar air heaters absorb the incoming solar radiation and transfer the heat energy to a fluid flowing through the collector. These have found several applications including space heating and crop drying. The efficiency of conversion of incident solar radiation to useful heat energy greatly depends upon effectiveness with which absorber surface transfers the heat to the working fluid. The efficiency of solar air heaters is found to be low because of low convective heat transfer coefficient of the flowing air inside the duct. The absorbed radiation energy by the absorber plate is not completely utilized by the air and leads to energy loss. Fins, artificial roughness on absorber surface and packed beds in the ducts are proposed for the enhancement of thermal performance of the collectors. In this paper V-shaped repeated rib roughness on the absorber plate is used for improving the performance of solar air heater.
The parameters influencing the heat transfer characteristics are Reynolds number (Re), Angle of attack of flow ($\alpha$), Relative roughness pitch (p/e), Relative roughness height (e/$D_h$) and the Aspect ratio (W/B) of the air heater duct. In this study ribs of various parameters are used as artificial roughness on absorber plate and performance of the air heater is investigated. Also investigations are carried out to develop a systematic approach for the selection of an optimum design for artificially roughened surface, which improves the heat transfer and reduces the pumping power. Experimental setup is fabricated and tests are

conducted to determine the effect of geometrical parameters of V-shaped wire ribbed absorber plate on heat transfer and friction characteristics.

Abdul-Malik et al. [1] carried out experimental investigation of the effect of geometrical parameters of V-shaped ribs on heat transfer and fluid flow characteristics of rectangular duct of solar air heater with absorber plate having V-shaped ribs on its underside. In this study rectangular duct is used where top absorber plate surface is artificially roughened using copper wires and other three surfaces were smooth and insulated. Also, correlations for heat transfer and friction factor for fully developed turbulent flow in a solar air heater duct were developed based on similarity laws. The results of expressions were compared with experimental results. They found increase in both Nusselt number and friction factor with increase in roughness height.

J.C. Han [2] carried out an experimental study of fully developed turbulent air flow in square ducts with two opposite rib roughened walls was performed to determine the effects of the rib pitch to height and rib height to equivalent diameter rations on friction factor and heat transfer coefficients. Reynolds number is varied from 7,000 to 90,000. Results of roughened wall were compared with those of smooth wall and observed that the average friction factor was 2.1 to 6 times that for four sides smooth duct. The Stanton number of the ribbed side is about 1.5 to 2.2 times that of the four-sided smooth duct when relative roughness pitch varies from 40 to 10. An experimental facility was constructed to determine the temperature variation and the increase in friction factor using uniformly heated plate with pin fins has been carried out. The collector had a rectangular shape with large width to gap ratio and one surface subjected to a uniform heat flux and other parallel plates perfectly insulated. Use of fins increases the collector efficiency. The collector with the fins collected 11% more energy than the collector without fins. But this was accompanied by significant increase in pressure drop. R.L. Webb and E.R.G. Eckert [3] conducted a comparative study between the roughened tubes and smooth tubes in design of heat exchangers. This study is conducted mainly to achieve enhancement of heat transfers capacity and also to reduce the friction factor.

Webb et al. [4] developed heat transfer and friction correlations for turbulent flow in tubes having repeated rib roughness. The friction correlation is based on *"Law of the wall similarity"*. The heat transfer correlation is based on application of a heat momentum transfer analogy to flow over a rough surface. The correlations are verified with experimental data taken with relative roughness height 0.01 to 0.04 and relative roughness pitch 10 to 40 and Prandtl number 0.71 to 37.6. Their work shows that law of the wall similarity adequately correlates the repeated rib heat transfer data over a wide range of relative roughness pitch, relative roughness height and Prandtl number. N. Sheriff and P. Gumley [5] investigated experimentally the heat transfer and friction characteristics of a surface with discrete roughness. They used metal wires as roughness elements of different sizes varying in a wide range of diameter. In this study they kept relative roughness pitch in the range 10:1. In this study it is shown that pumping power required to force the fluid for same heat transfer surface and fluid temperature difference, will be minimum when $(f_r/f_s) < (Nu_r/Nu_s)^3$. This shows any increase in the friction factor increases the heat transfer characteristics of roughened surface resulting in a more efficient heat transfer surface.

E.M.Sparrow and L.M. Hossfeld [6] conducted experiments to determine the heat transfer, pressure drop and flow field responses to the rounding of the peaks of a corrugated wall duct. The experiments cover the range of Reynolds numbers 2,000 to 33,000 and the Prandtl number 4 to 11. Results show that for a given Reynolds number there is decrease in both friction factor and Nusselt number for round corrugated peaks as compared to sharp peak corrugation. However, reduction in Nusselt number was found to be 8 to 18% while it was about 60% for friction factor. The effect of roundness was found to be more at higher Reynolds number.

J.C. Han et al. [7] studies effects of heat transfer and friction for rib roughened surfaces. This investigation was undertaken to determine shape, angle of attack and pitch to height ratio on friction factor and heat transfer. In this study parallel plate geometry based on law of wall of similarity is used. Correlation for friction factor and heat transfer was developed to account for rib shape, spacing and angle of attack. Ribs at 45$^o$ angle of attack were found to have superior heat transfer performance at a given friction power when compared to ribs at a 90$^o$ angle of attack of flow or when compared to sand grain roughness. D.L. Gee and R.L. Webb [8] contributed experimental information for single phase forced convection in circular tube containing a two dimensional rib roughness. They conducted experiments and provided reports of heat transfer and friction characteristics for air flow with three helix angles (30$^o$, 49$^o$ and 70$^o$) all having a rib pitch to height ratio of 15. They preferred helix angle is approximately 45$^o$ because it offers the superior performance.

M.J. Lewis [9] carried out an elementary analysis for predicting the momentum and heat transfer characteristics of a hydraulically rough surface. In this study equally spaced rectangular ribs are considered. This work provides quick and simple method of evaluating or optimizing rough surfaces.

R.P. Saini and Jitendra Verma [10] developed heat transfer and friction factor correlations for a duct having dimple shape artificial roughness on the underside of the absorber surface. The maximum value of Nusselt number has been found corresponds to relative roughness height ($e/D_h$) of 0.0379 and relative pitch ($p/e$) of 10. While minimum value of friction factor has been found correspond to relative roughness height ($e/D_h$) of 0.0289 and relative pitch ($p/e$) of 10. It is therefore suggested that, roughness parameters of the geometry are to be selected by considering the net heat gain and corresponding power required to force the air through the duct.

Santosh B. Bopche and Madhukar S. Tandale [11] investigated heat transfer and frictional characteristics of a turbulator roughened solar air heater duct. Enhancement in the heat transfer and friction factor by 2.82 and 3.72 times, were reported respectively in the turbulator roughened duct. It is shown that maximum heat transfer enhancement can be achieved at affordable friction price. Sahu and Bhagoria [12] have investigated the effect of $90^o$ broken wire ribs on heat transfer coefficient of a solar air heater duct. A pitch of 20 mm gives the highest thermal efficiency of 83.5% for and element height of 1.5 mm and reported heat transfer coefficient of roughened duct is 1.25 to 1.4 times compared to smooth duct under similar operating conditions at higher Reynolds number.

Many investigators [13-19] conducted experimental study on heat transfer and friction in solar air heater ducts with different types of roughness on the absorber plate. Performance of roughened absorber air heater was better compared to that of having smooth absorber plate.

The present investigation was, therefore, carried out with the objective of extensive experimentation in order to increase the heat transfer in solar air heater ducts with artificial roughness is the form of repeated ribs on the absorber plate.

## 2. Experimental details

### 2.1 Experimental setup

A schematic diagram of experimental setup is shown in Figure 1. It consists of smooth entrance section, roughened entrance section, test section, an exit section, mixing chamber, a flow meter and an air blower. The duct size is 2600mm × 150mm × 30mm (dimensions of the inner cross section) made of wooden panels. Test section length is 1200mm. The length of smooth entrance section and exit section are 800mm and 600mm respectively. For a roughened duct thermally fully developed flow will be established in a short length i.e 2–3 times of hydraulic diameter therefore short entrance length is chosen. For the turbulent flow regime, the lengths are considered as per ASHRAE standard 93–97 [20]. A 2–mm thick aluminium sheet of 1200mm × 150mm size is used as an absorber plate and the lower surface of the plate provided with artificial roughness in the form of V-shaped copper wires of various values of pitch and angle of attack of flow. Relative roughness pitch of the roughness elements is varied from 10 to 40 and relative roughness height is varied from 0.01 to 0.04. A solar simulator is used as heater to provide a uniform heat flux up to a maximum of 1500 W/m$^2$ to the absorber plate. It consists of five electric bulbs of 100 Watt each. These bulbs are equally spaced and kept on the absorber plate to provide uniform heating and to simulate the solar radiation flux. The power supply to the heater is controlled through an AC variac. The duct is insulated on the other three sides except absorber plate side to ensure all the heat flux is transferred to the duct and also to minimize the heat loss. Aluminium wires as roughness elements are pasted below the absorber plate in the form of V-shape. The air flow rate in the duct is measured by means of an orifice meter connected with an U–tube manometer. The other end of the duct is connected to a circular pipe via a rectangular to circular transition section. Calibrated chromel–alumel thermocouples are used to measure air and absorber plate temperatures at various locations. The pressure drop across the test section is measured with the help of a micro–manometer.

### 2.2 Instrumentations

#### 2.2.1 Temperature measurement

Calibrated chromel–alumel thermocouples with digital temperature indicator, indicating output in degree centigrade with an accuracy of 0.1 $^o$C through a selector switch are used to measure air and absorber plate temperatures at various locations. Eight thermocouples are pasted on the top surface of the absorber plate to record the plate temperature. The locations of thermocouples on absorber plate

are shown in Figure 2(a). The air temperature inside the duct is recorded using ten thermocouples inserted inside the duct at different locations as shown in Figure 2(b). Also, an inlet and outlet temperature of air is measured by two separate thermocouples.



1.  AIR INLET
2.  ENTRANCE SECTION
3.  TEST SECTION
4.  HEATER (SOLAR SIMULATOR)
5.  EXIT SECTION AND MIXING CHAMBER
6.  TRANSITION SECTION
7.  ORIFICE METER
8.  U–TUBE MANOMETER
9.  GATE VALVE
10. BLOWER
11. AIR OUTLET
12. ELECTRICAL MOTOR
13. POWER SUPPLY TO MOTOR
14. MICROMANOMETER
15. SELECTOR SWITCH
16. DIGITAL TEMPERATURE INDICATOR
17. POWER SUPPLY TO HEATER
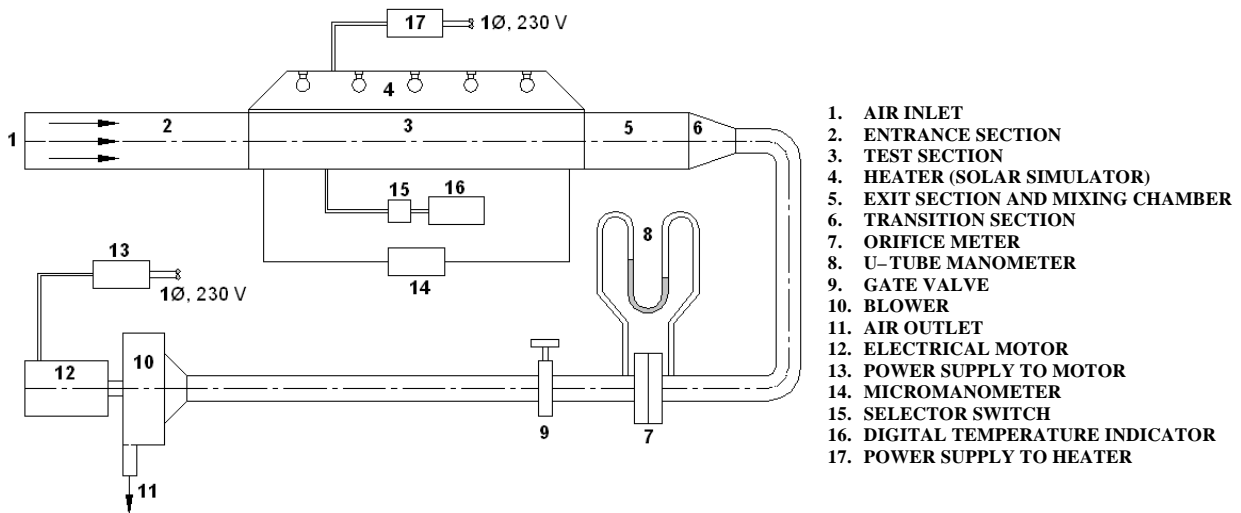
Figure 1. Schematic diagram of experimental setup



All dimensions are in mm
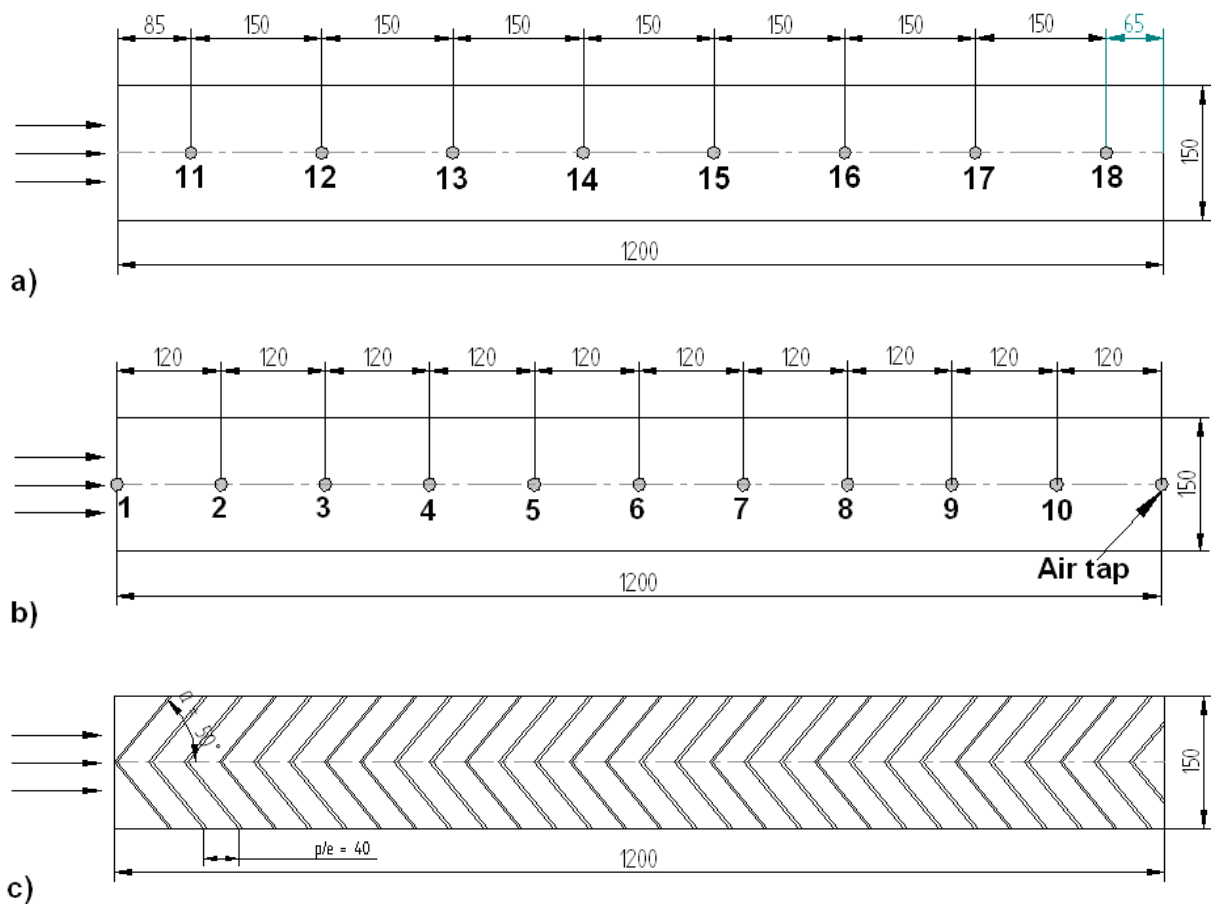
Figure 2. (a) Position of the thermocouples on the absorbing plate (test length); (b) Position of the thermocouples in the air duct (test length); (c) Schematic diagram of V-shape wire roughness geometry on the absorber plate

*2.2.2 Air flow measurement*
The air is sucked through the rectangular duct by means of a blower. Control valve is used to control the air flow rate through the duct. The air is thoroughly mixed in the mixing chamber consisting of baffles and the temperature is measured at the exit. The air flow rate in the duct is measured by means of a flange type orifice meter calibrated by using pitot tube. Pressure drop is measured by a U–tube manometer connected across the orifice meter with water as manometric fluid.

*2.2.3 Pressure drop measurement in the duct*
The pressure drop in the test section is measured by a micro–manometer with a least count of 0.005mm. The micro manometer consists of a relatively large reservoir of fluid connected through a flexible hose to a glass tube that is inclined at an angle of about five degrees from the horizontal. Inclined glass tube is mounted on a sliding arrangement with a screw having a pitch of 1.8mm and a graduated dial having 360 divisions, each division showing a movement of 0.005 mm of the reservoir. The meniscus of the liquid in glass tube is maintained at a fixed prescribed mark by sliding the tube up or down. This movement is noted which yield the pressure difference across the two pressure tapping. The pressure tapping fixed at outlet of the test length is connected to the reservoir of the micro–manometer. The butyl alcohol having specific gravity 0.8 has been used in the manometer to increase the accuracy further.

*2.3 Roughness geometry and range of parameters*
V-shaped wire roughness geometry on the absorber plate which is investigated under the present investigation is shown in Figure 2(c). The Range of parameters covered under the present experimental study is as follows:
(i)    Reynolds number $2{,}500 \leq Re \leq 8{,}500$.
(ii)   Angle of attack of flow $20^o \leq \alpha \leq 90^o$.
(iii)  Relative roughness pitch $10 \leq p/e \leq 40$.
(iv)   Relative roughness height $0.01 \leq e/D_h \leq 0.04$.

## 3. Experimental procedure
Before starting the experiment all the components of the setup and instruments viz. micro–manometer, U–tube manometer, voltmeter, ammeter and thermocouples are checked carefully for their proper operation. Ribbed absorber plate is installed and the test section is assembled.
The energy for heating is supplied by the heater for one hour to the test section. After one hour the blower is then switched on ensuring no leakage in the joints of the duct and pressure tappings. The mass flow rate in the duct is adjusted using control valves. Once the mass flow rate of air is fixed, all the readings are taken when the system attains quasi–steady state. Quasi–steady state means that the temperatures do not change appreciably for 10–15 min. It is decided to conduct tests for fourteen values of mass flow rate of air in order to cover the entire range of Reynolds number.
The following parameters are measured during experimentation:
(i)     Temperature of the absorber plate at various locations.
(ii)    Temperature of the air at inlet and outlet.
(iii)   Temperature of the air at various locations of the test section.
(iv)    Pressure difference across the orifice meter.
(v)     Pressure drop across the test section.
(vi)    Voltage and current supply to the heater.

## 4. Data reduction
Steady state values of the plate and air temperatures in the duct at various locations were obtained for a given heat flux and mass flow rate of air. These values were used to compute heat transfer rate to the air flowing in the duct. Nusselt number and friction factor were also calculated to know the effect of roughness geometry and operating parameters on heat transfer and friction characteristics. The following expressions were used for the calculation of mass flow rate (m), velocity of air (V), heat supplied to the air (q), and heat transfer coefficient (h).

$$m = \rho C_d a_o \sqrt{\frac{2gH}{1-(a_o/a_1)^2}} \tag{1}$$

The calibration of orifice plate is done against a standard pitot tube which gives a value of 0.62 for coefficient of discharge ($C_d$). Where, $H = h_m(\rho_w/\rho)$ and ($h_m$) is manometer reading. The velocity of air in the duct is calculated as follows.

$$V = \frac{m}{\rho W B} \tag{2}$$

Useful heat gain to the air flowing in the duct is calculated as follows.

$$q = m C_p (t_o - t_i) \tag{3}$$

The temperature $t_o$ and $t_i$ are values of the air inlet and outlet temperatures respectively. Convective heat transfer coefficient for the test section is calculated as follows.

$$h = \frac{q}{A_c(t_p - t_f)} \tag{4}$$

where, ($A_c$) is the area of absorber plate, the temperature ($t_p$) and ($t_f$) are average values of the absorber plate and fluid (air) temperature, respectively.
The convective heat transfer coefficient was then used to obtain the average Nusselt number from the following expression.

$$Nu_r = \frac{hD_h}{k} \tag{5}$$

The friction factor was determined from the measured values of pressure drop across the test length, L = 1000mm using following expression.

$$f_r = \frac{D_h \Delta p}{2LV^2\rho} \tag{6}$$

The experimental setup was verified by conducting validity tests for smooth duct under similar conditions.
The values of Nusselt number and friction factor were determined for smooth duct and compared with the values obtained from correlations of Dittus–Boelter equation for the Nusselt number and modified Blasius equation for the friction factor [10].
Nusselt number for a smooth rectangular duct is given by Dittus-Boelter equation [11] as

$$Nu_s = 0.023 \mathrm{Re}^{0.8} \mathrm{Pr}^{0.4} \tag{7}$$

Friction factor for a smooth rectangular duct is given by the Modified Blasius equation [11] as

$$f_s = 0.0791 \mathrm{Re}^{-0.25} \tag{8}$$

## 5. Error analysis
An error analysis of experimental measurements has been carried out on the basis of method proposed by Kline and McClintock [21]. This method was used for the prediction of uncertainty which should be associated with an experimental result based on observations of the scatter in the raw data used in calculating the result. The maximum possible measurement errors in the values of major parameters of present investigation are given below.

(i)    Reynolds number = ±4.53%
(ii)   Heat transfer coefficient = ±2.57%
(iii)  Nusselt number = ±4.91%
(iv)   Friction factor = ±4.77%

## 6. Results and discussion

The values of Nusselt number and friction factor for V-shaped wire roughness geometry were computed on the basis of experimental data collected for various flow and roughness parameters. The effects of various parameters on Nusselt number and friction factor are presented in this section.

Variation of absorber plate temperature and fluid temperature in the duct is shown in Figure 3. The temperatures tp and tf are the average values of absorber plate temperature and fluid temperature respectively. The average value of plate temperature was determined from eight thermocouples readings at different locations on the absorber plate as shown in Figure 2(a). The average value of fluid temperature was found from the readings of ten thermocouples fixed in central locations of the duct cross-section along the flow direction. It was found that in the span wise direction the variation of temperature was negligible. This variation of temperature is in agreement with work of Abdul-Malik et al. [1]. Comparison of experimental and predicted values of Nusselt number and friction factor are shown in Figures 4 and 5. A reasonable good agreement between the experimental and predicted data ensures accuracy of the data being collected with the help of experimental setup. Nusselt number and friction factor of smooth duct proposed by modified Dittus-Boelter correlation for Nusselt Number and by modified Blasius Correlation for friction factor.
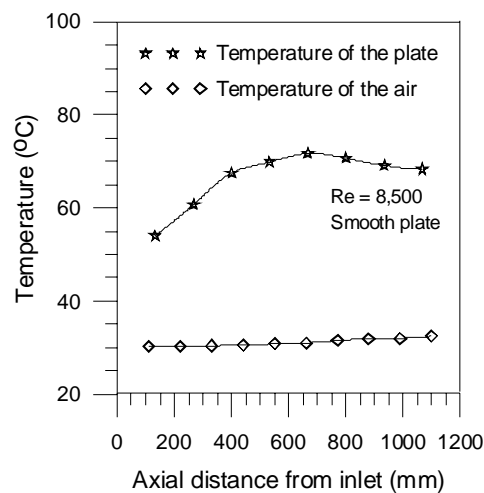


Figure 3. Plate and air temperature distribution along the length of the test duct
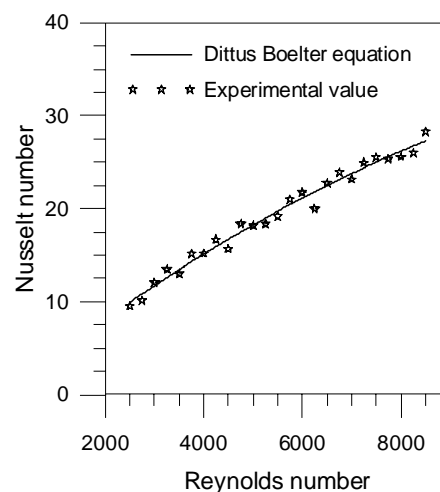


Figure 4. Comparison of experimental values and predicted values of Nusselt number for smooth duct
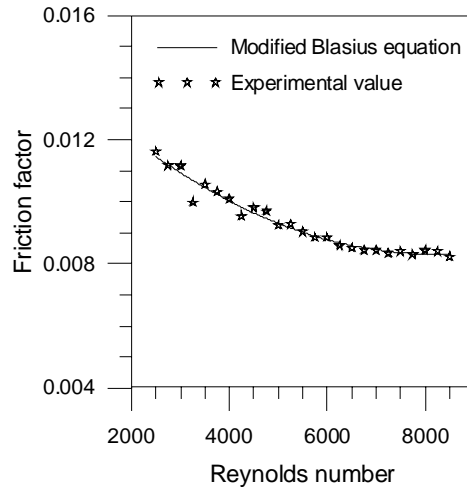
Figure 5. Comparison of experimental values and predicted values of friction factor for smooth duct

*6.1 Effect of Reynolds number*
Figure 6 illustrates the effect of Reynolds number on Nusselt number for various values of relative roughness pitch (p/e) and other parameters i.e. relative roughness height (e/Dh) of 0.04 and angle of attack of flow (α) of 90o. Figure 7 illustrates the effect of Reynolds number on Nusselt number for various values of relative roughness height (e/Dh) and other parameters i.e. relative roughness pitch (p/e) of 10 and angle of attack of flow (α) of 50o. It is observed from Figures 6 and 7 that for given values of roughness parameters, Nusselt number increases monotonously with an increase in Reynolds number. The values of Nusselt number for roughened absorber plate are considerably higher as compared to smooth one for a given Reynolds number.

Figure 8 illustrates the effect of Reynolds number on friction factor for various values of relative roughness pitch (p/e) and other parameters i.e. relative roughness height (e/Dh) of 0.04 and angle of attack of flow (α) of 90o. Figure 9 illustrates the effect of Reynolds number on friction factor for various values of relative roughness height (e/Dh) and other parameters i.e. relative roughness pitch (p/e) of 10 and angle of attack of flow (α) of 50o. It is observed from Figures 8 and 9 that for given values of roughness parameters, Nusselt number increases whereas the friction factor decreases with and increase of Reynolds number. However, the values of Nusselt number and friction factor are different as compared to those obtained for smooth absorber plates. This is due to a distinct change in the fluid flow characteristics as a result of roughness that causes flow separations, reattachments and the generation of secondary flows.
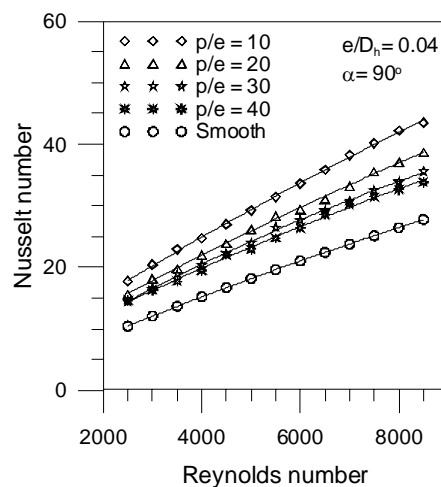


Figure 6. Variation of Nusselt number with Reynolds number for different values of relative roughness pitch (p/e)
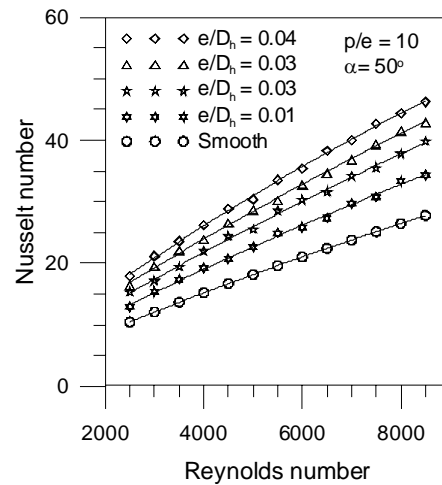
Figure 7. Variation of Nusselt number with Reynolds number for different values of relative roughness height (e/D$_h$)
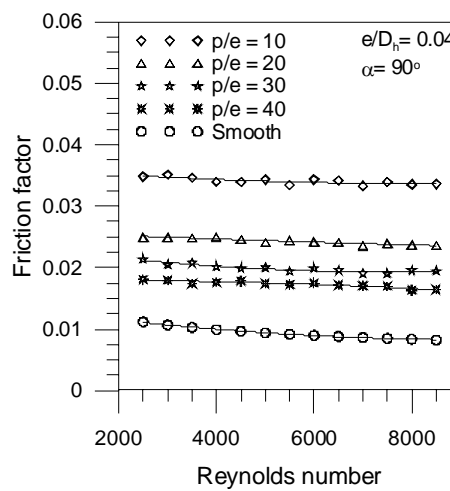


Figure 8. Variation of friction factor with Reynolds number for different values of relative roughness pitch (p/e)
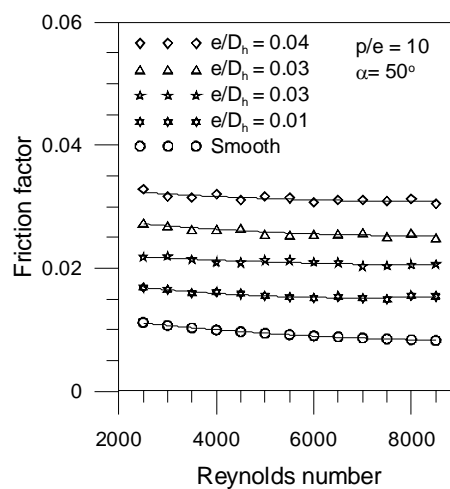


Figure 9. Variation of friction factor with Reynolds number for different values of relative roughness height (e/D$_h$)

*6.2 Effect of relative roughness pitch*
Figure 10 illustrates the effect of relative roughness pitch (p/e) on Nusselt number for various values of Reynolds number and other parameters i.e. relative roughness height (e/Dh) of 0.01 and angle of attack of flow (α) of 90o. In this case Nusselt number is observed to decrease with increase in relative roughness pitch (p/e). This is due to the fact that with the increase in relative roughness pitch, number of reattachment points over the absorber plate reduces. Therefore, relative roughness pitch value should be taken less so that number of reattachment points increases and augmentation in heat transfer takes place but it has also been seen that the value of relative roughness pitch should not be less than eight [4], in this case reattachment point could not form. In this study, it has been observed that maximum value of Nusselt number is obtained for relative roughness pitch (p/e) value of 10.

*6.3 Effect of relative roughness height*
Figure 11 illustrates the effect of relative roughness height (e/Dh) on Nusselt number for various values of Reynolds number and other parameters i.e. relative roughness pitch (p/e) of 10 and angle of attack of flow (α) of 90o. It can be observed that the increase in relative roughness height results in an increase in Nusselt number and very larger relative roughness height might produce the same effect as that of relative roughness pitch less than 8. In this study, it has been observed that maximum value of Nusselt number is obtained for relative roughness height (e/Dh) value of 0.04.
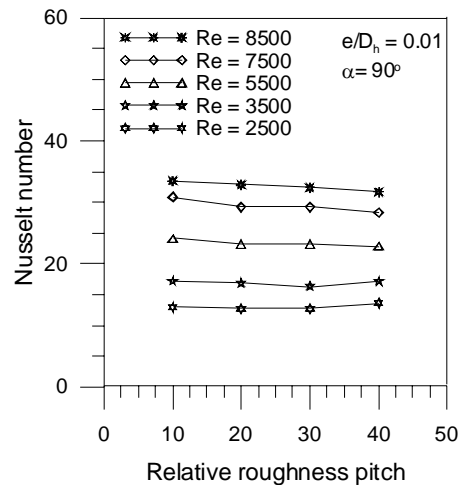
Figure 10. Variation of Nusselt number with relative roughness pitch (p/e) for different values of Reynolds number
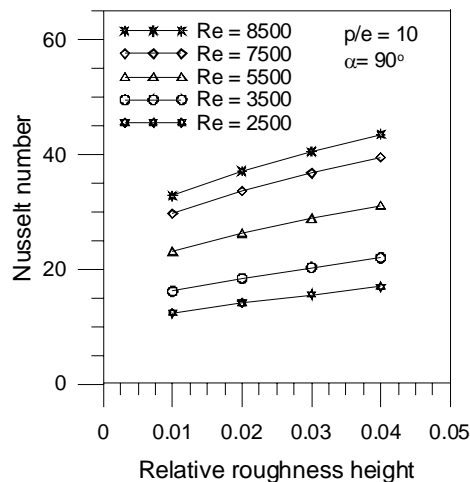
Figure 11. Variation of Nusselt number with relative roughness height (e/D$_h$) for different values of Reynolds number

*6.4 Effect of angle of attack of flow*

Figure 12 illustrates the effect of angle of attack of flow (α) on Nusselt number for various values of Reynolds number and other parameters i.e. relative roughness pitch (p/e) of 10 and relative roughness height (e/Dh) of 0.01. It appears from this figure that initially any increase in the angle of attack of flow improves the heat transfer characteristics and maximum Nusselt number occurs in the range of 50o-60o. Further any increase in angle of attack of flow reduces the Nusselt number. The reason for the occurrence of these maxima at 50o-60o angle of attack of flow range is yet to be investigated in detail.
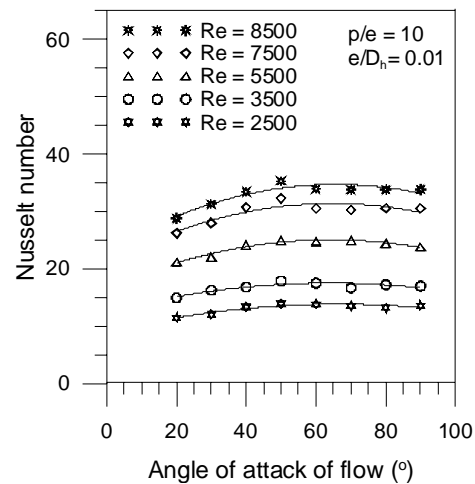


Figure 12. Variation of Nusselt number with angle of attack (α) for different values of Reynolds number

## 7. Thermo-hydraulic performance

It has been found that the artificial roughness on the absorber plate of the roughened duct results in considerable enhancement of heat transfer. This enhancement is, however, accompanied by a substantial increase in friction factor. It is, therefore, desirable that to select the roughness geometry such that the heat transfer is maximized while keeping the friction losses at the minimum possible value. This requirement of the collector can be fulfilled by considering the heat transfer and friction characteristics simultaneously. A parameter that facilitates the simultaneous consideration of thermal and hydraulic performance is given by Webb and Eckert [3] as $(Nu_r/Nu_s)/(f_r/f_s)^{1/3}$. This parameter is plotted in Figure 13 against Reynolds number for relative roughness pitch (p/e) of 10, relative roughness height (e/D$_h$) of 0.04 and for different angles of attack (α).
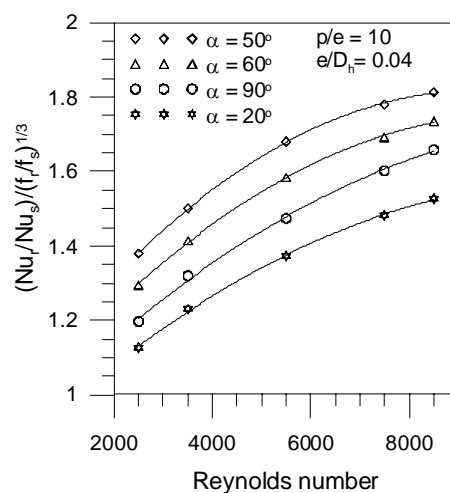


Figure 13. Variation of performance parameter with Reynolds number for different values of angle of attack of flow (α)

Figure 14 shows the variation of performance parameter against Reynolds number for relative roughness pitch (p/e) of 10, angle of attack of flow (α) of 50o and for different values of relative roughness height (e/Dh).
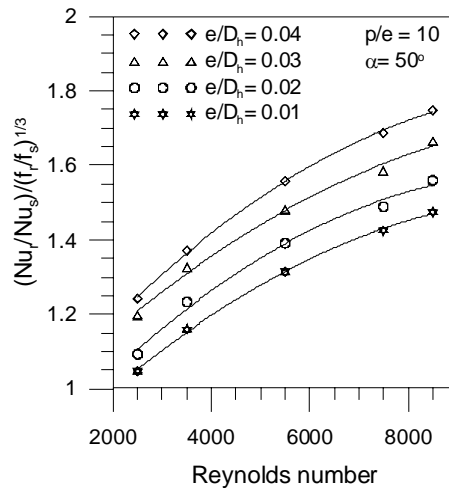


Figure 14. Variation of performance parameter with Reynolds number for different values of relative roughness height (e/D$_h$)

Also it was found that as the relative roughness height is varied, the value of this performance parameter in general increases with an increase of relative roughness height in the range of values investigated. The value of this parameter greater than unity indicates it is overall advantageous to use roughened duct in comparison with smooth duct.

## 8. Correlations for Nusselt number and friction factor
From Figures 6-12, it can be concluded that Nusselt number and friction factor are strong functions of flow and roughness parameters, namely Reynolds number (Re), relative roughness pitch (p/e), relative roughness height (e/Dh) and angle of attack of flow (α). The functional relationships for Nusselt number and friction factor can therefore be written as:

$$Nu = f(\text{Re}, p/e, e/D_h, \alpha) \tag{9}$$

$$f_r = f(\text{Re}, p/e, e/D_h, \alpha) \tag{10}$$

In order to obtain the performance of an artificially roughened duct having V shaped wires as roughness geometry, Nusselt number and friction factor correlation were developed for operating parameters by following the procedure reported by Abdul-Malik [1].

### 8.1 Correlation for Nusselt number
The data corresponding to all the 10 roughened plates totaling 338 data points were used for regression analysis to fit a second order polynomial. The data points of Nusselt number from experimental data were plotted against Reynolds number as shown in Figure 15. A regression analysis to fit a straight line through these data points may be represented as:

$$Nu_r = A_0 (Re)^{0.7618} \tag{11}$$

The coefficient A0 will be a function of other influencing parameters. Now, taking the parameter relative roughness pitch (p/e) into consideration, the value of $\left[ \left( N_{u_r}/(\text{Re})^{0.7618} \right) = A_0 \right]$ corresponding to all values of pitch (p/e) is plotted against pitch (p/e) as shown in Figure 16.

Regression analysis to fit a second-order quadratic curve fit may be represented by the following expression:

$$log\left(\frac{Nu_r}{Re^{0.7618}}\right) = log\,B_0 + B_1\left(log\left(\frac{p}{e}\right)\right) + B_2\left(log\left(\frac{p}{e}\right)\right)^2$$

(12)

The above equation can be rearranged as:

$$\left(\frac{Nu_r}{Re^{0.7618}}\right) = B_0\left(\frac{p}{e}\right)^{0.0007}\left(exp(0.000008)\left(log\left(\frac{p}{e}\right)\right)^2\right)$$

(13)
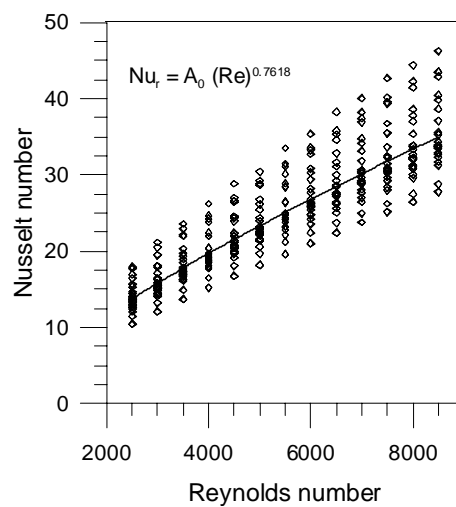


Figure 15. Plot of Nusselt number versus Reynolds number for 338 data points
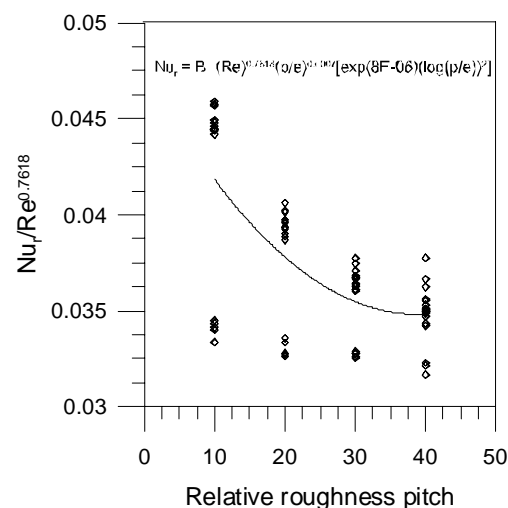


Figure 16. Plot of $(Nu_r/Re^{0.7618})$ versus relative roughness pitch

Further, the constant $B_o$ will be the function of relative roughness height $(e/D_h)$.

$$\left[\frac{\left(\dfrac{Nu_r}{Re^{0.7618}}\right)}{\left(\dfrac{p}{e}\right)^{0.0007}\left(exp(0.000008)\left(log\left(\dfrac{p}{e}\right)\right)^2\right)}\right] = B_0$$

(14)

A plot of Bo versus relative roughness height (e/Dh) has been drawn as shown in Figure 17. A second-order quadratic curve fit in the following form is obtained.

$$log\left(\frac{\left(\dfrac{Nu_r}{Re^{0.7618}}\right)}{\left(\dfrac{p}{e}\right)^{0.0007}\left(exp(0.000008)\left(log\left(\dfrac{p}{e}\right)\right)^2\right)}\right) = log\,C_0 + C_1\left(log\left(\dfrac{e}{D_h}\right)\right) + C_2\left(log\left(\dfrac{e}{D_h}\right)\right)^2$$

(15)

The above equation can be rearranged as:

$$\left(\frac{\left(\dfrac{Nu_r}{Re^{0.7618}}\right)}{\left(\dfrac{p}{e}\right)^{0.0007}\left(exp(0.000008)\left(log\left(\dfrac{p}{e}\right)\right)^2\right)}\right) = C_0\left(\dfrac{e}{D_h}\right)^{0.5919}\left(exp(-3.5388)\left(log\left(\dfrac{e}{D_h}\right)\right)^2\right)$$

(16)

Further, the constant C0 will be the function of angle of attack of flow (α).

$$\left(\frac{\left(\dfrac{Nu_r}{Re^{0.7618}}\right)}{\left(\dfrac{p}{e}\right)^{0.0007}\left(exp(0.000008)\left(log\left(\dfrac{p}{e}\right)\right)^2\right)\left(\dfrac{e}{D_h}\right)^{0.5919}\left(exp(-3.5388)\left(log\left(\dfrac{e}{D_h}\right)\right)^2\right)}\right) = C_0$$

(17)

A plot of Co angle of attack of flow (α) has been drawn as shown in Figure 18. A second-order quadratic curve fit in the following form is obtained.

$$log\left(\frac{\left(\dfrac{Nu_r}{Re^{0.7618}}\right)}{\left(\dfrac{p}{e}\right)^{0.0007}\left(exp(0.000008)\left(log\left(\dfrac{p}{e}\right)\right)^2\right)\left(\dfrac{e}{D_h}\right)^{0.5919}\left(exp(-3.5388)\left(log\left(\dfrac{e}{D_h}\right)\right)^2\right)}\right) = log\,D_0 + D_1(log(\alpha)) + D_2(log(\alpha))^2$$

(18)

The above equation can be rearranged as:

$$\left[ \frac{\left( \dfrac{Nu_r}{Re^{0.7618}} \right)}{\left( \dfrac{p}{e} \right)^{0.7618} \left( \exp(0.000008) \left( \log\left( \dfrac{p}{e} \right) \right)^2 \right) \left( \dfrac{e}{D_h} \right)^{0.5919} \left( \exp(-3.5388) \left( \log\left( \dfrac{e}{D_h} \right) \right)^2 \right)} \right] = D_0 (\alpha)^{0.0465} \left( \exp(-0.0004)(\log(\alpha))^2 \right)$$

(19)

The values of the coefficients are obtained as given below:
A0=0.0355, B0=0.0475, C0=0.0289, D0=3.1106
These values result in the following correlation for Nusselt number:

$$Nu_r = 3.1106 Re^{0.7618} \left( \frac{p}{e} \right)^{0.7618} \left( \exp 0.000008 \left( \log\left( \frac{p}{e} \right) \right)^2 \right) \times \left( \frac{e}{D_h} \right)^{0.5919} \left( \exp(-3.5388) \left( \log\left( \frac{e}{D_h} \right) \right)^2 \right) \times (\alpha)^{0.0465} \left( \exp(-0.0004)(\log(\alpha))^2 \right)$$ (20)

Figure 19 shows the comparison between the experimental values of Nusselt number and those of predicted by the correlation developed for Nusselt number. The data points of Nusselt number lie within the deviation lines of ±10%.
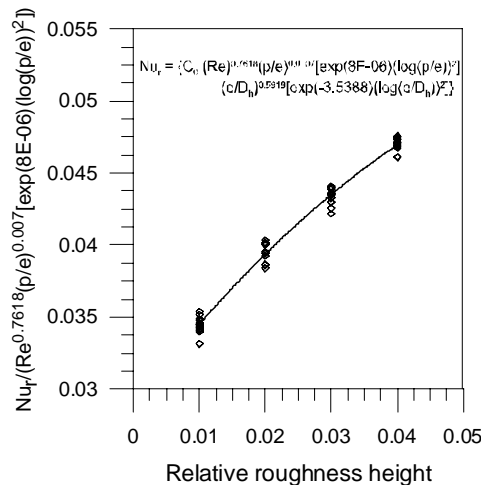


Figure 17. Plot of $(Nu_r/(Re^{0.7618}(p/e)^{0.007} [\exp(8E-06) (\log(p/e))^2]))$ versus relative roughness height
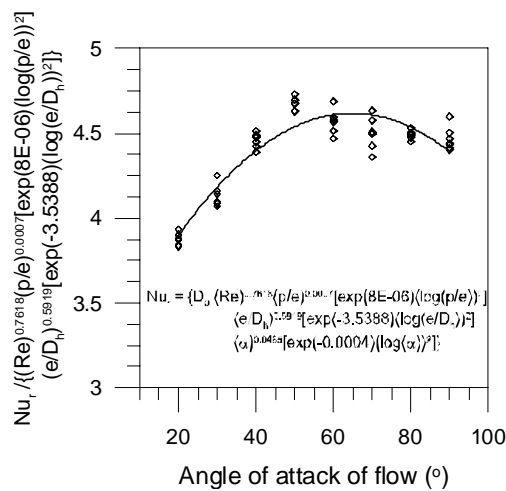


Figure 18. Plot of $(Nu_r /\{(Re)^{0.7618}(p/e)^{0.0007} [\exp(8E-06) (\log(p/e))^2](e/D_h)^{0.5919} [\exp(-3.5388) (\log(e/D_h))^2]\})$ versus angle of attack of flow
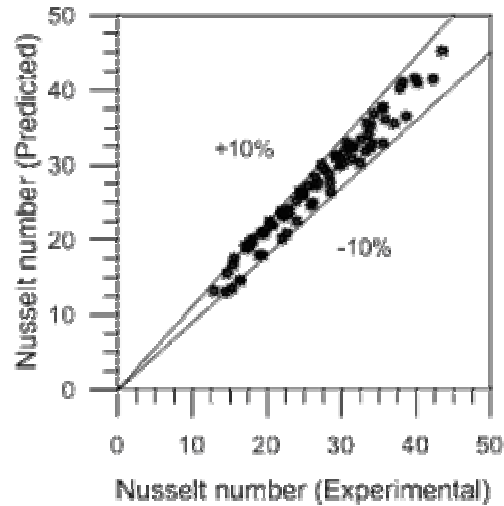
Figure 19. Comparison of predicted and experimental values of Nusselt number

*8.2 Correlation for friction factor*
A similar procedure has been employed to develop correlation for friction factor as shown in Figures 20-23. The final form of correlation for friction factor is obtained as follows.

$$f_r = (0.004)\,\mathrm{Re}^{-0.05}\left(\frac{p}{e}\right)^{-0.002}\left(\exp(0.00003)\left(\log\left(\frac{p}{e}\right)\right)^2\right)\times \left(\frac{e}{D_h}\right)^{0.236}\left(\exp(0.85)\left(\log\left(\frac{e}{D_h}\right)\right)^2\right)\times (\alpha)^{0.0001046}\left(\exp(0.000001)(\log(\alpha))^2\right) \quad (21)$$

Figure 24 shows the comparison between the experimental values of friction factor and those of predicted by the correlation developed for friction factor. The data points of friction factor lie within the deviation lines of ±10%. Hence, the correlations developed are reasonably satisfactory for the prediction of the Nusselt number and friction factor of V- shaped wire roughened duct with fairly good accuracy in the range of parameters investigated.
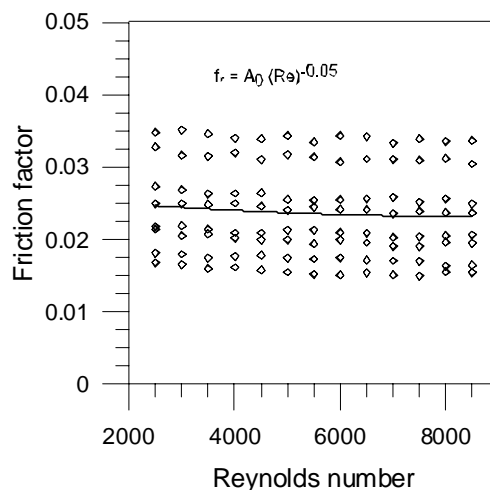


Figure 20. Plot of friction factor versus Reynolds number for 104 data points
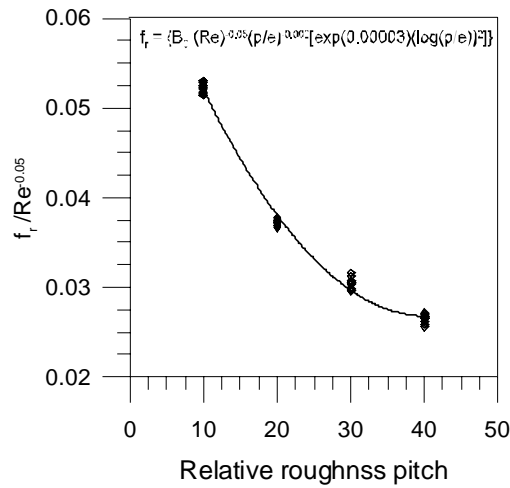
Figure 21. Plot of $(f_r /(Re)^{-0.05})$ versus relative roughness pitch
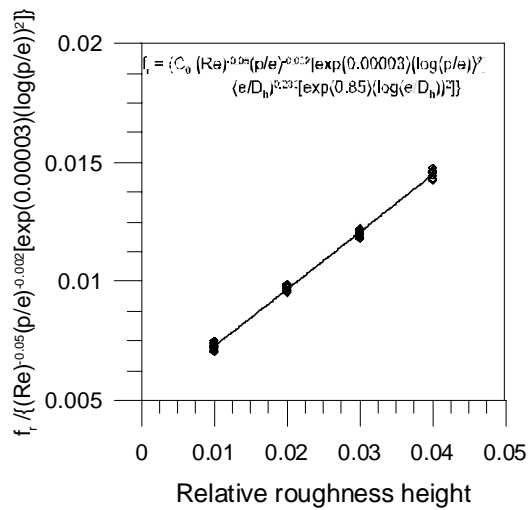


Figure 22. Plot of $(f_r /\{(Re)^{-0.05}(p/e)^{-0.002}[exp(0.00003)\ (log(p/e))^2]\})$ versus relative roughness height
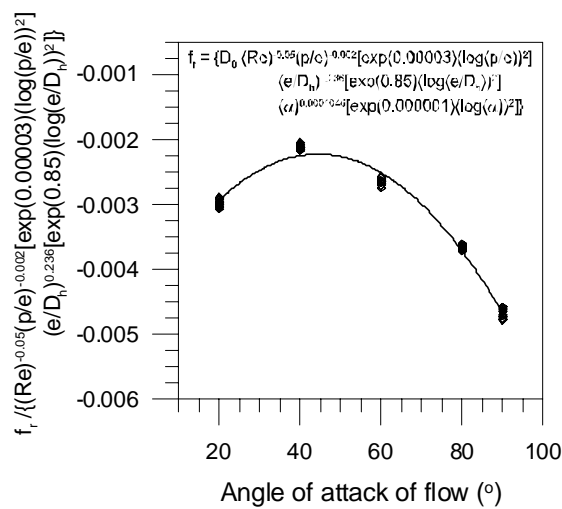


Figure 23. Plot of $(f_r /\{(Re)^{-0.05}(p/e)^{-0.002}\ [exp(0.00003)\ (log(p/e))^2]\ (e/D_h)^{0.236}\ [exp(0.85)\ (log(e/D_h))^2]\})$ versus angle of attack of flow

Figure 24. Comparison of predicted and experimental values of friction factor

## 9. Conclusion

An extensive investigation has been carried out with an intention to develop a systematic approach for the selection of an optimum design for artificially wire roughened surface, which improves heat transfer characteristics as well as reduces the pumping power requirement.

The following conclusions can be drawn from this work:

a) In general, Nusselt number increases and friction factor decreases with an increase of Reynolds number. Nusselt number and friction factor are significantly higher as compared to those obtained for smooth absorber plates. This is due to the distinct change in the fluid flow characteristics as a result of roughness that causes flow separations, reattachments and the generation of secondary flows.

b) The maximum value of Nusselt number has been found corresponds to relative roughness height ($e/D_h$) of 0.04 and relative roughness pitch (p/e) of 10. While minimum value of friction factor has been found corresponds to relative roughness height ($e/D_h$) of 0.01 and relative roughness pitch (p/e) of 40. Its is therefore, roughness parameters of the geometry can be selected by considering net heat gain and corresponding pumping power required to drive the air through the duct.

c) The roughness parameter angle of attack of flow has also been considered. From analysis it has been observed that maximum value of Nusselt number is obtained for the range of 50°-60° angle of attack of flow. For all the values of relative roughness height and relative roughness pitch considered.

d) In this study it is shown that pumping power required to force the fluid for same heat transfer surface and fluid temperature difference, will be minimum when, $(f_r/f_s) < (Nu_r/Nu_s)^3$. This shows any increase in the friction factor increases the heat transfer characteristics of roughened surface resulting in a more efficient heat transfer surface.

e) The maximum enhancement in Nusselt number and friction factor values compared to smooth duct are of the order of 1.5 and 2.7 respectively.

It can therefore be concluded that the correlations are reasonably satisfactory for the prediction of Nusselt number and friction factor for the roughened duct.

## Nomenclature

$A_c$     Area of absorber plate (m$^2$)
$a_o$     Area of the orifice (m$^2$)
$a_1$     Area of the pipe (m$^2$)
B     Height of the duct (m)
$C_p$     Specific heat of air (J/kg K)
$C_d$     Coefficient of discharge (dimensionless)
$d_o$     Diameter of the orifice (m)
$d_1$     Diameter of the pipe (m)
$D_h$     Hydraulic diameter of duct (m)
e     Height of roughness element (m)
$e/D_h$     Relative roughness height (dimensionless)

| | |
|---|---|
| $f_r$ | Friction factor of roughened duct (dimensionless) |
| $f_s$ | Friction factor of smooth duct (dimensionless) |
| h | Convective heat transfer coefficient (W/m$^2$ K) |
| $h_m$ | Manometer reading (m) |
| k | Thermal conductivity of air (W/m K) |
| L | Test length (m) |
| m | Mass flow rate of air (kg/s) |
| $Nu_r$ | Nusselt number of roughened duct (dimensionless) |
| $Nu_s$ | Nusselt number of smooth duct (dimensionless) |
| p | Rib pitch (m) |
| p/e | Relative roughness pitch (dimensionless) |
| Pr | Prandtl number (dimensionless) |
| q | Rate of heat transfer to air (W) |
| Re | Reynolds number (dimensionless) |
| $t_i$ | Air inlet temperature ($^o$C) |
| $t_o$ | Air outlet temperature ($^o$C) |
| $t_f$ | Average temperature of fluid ($^o$C) |
| $t_p$ | Average temperature of absorbing plate ($^o$C) |
| V | Velocity of air in the duct (m/s) |
| W | Width of the duct (m) |
| W/B | Aspect ratio (dimensionless) |

*Greek symbols*

| | |
|---|---|
| $\Delta p$ | Pressure drop in the test length (N/m$^2$) |
| $\alpha$ | Angle of attack of flow (degree) |
| $\eta$ | Efficiency index |
| $\rho$ | Density of air (kg/m$^3$) |
| $\tau$ | Shear stress for duct (N/m$^2$) |

*Subscript*

| | |
|---|---|
| s | Smooth duct |
| r | Roughened duct |
| av | Average |

**References**

[1]    abdul-Malik Ebrahim Momin, J.S. Saini and S.C. Solanki, Heat transfer and friction in solar air heater duct with V-shaped rib roughness on absorber plate, International Journal of Heat and Mass Transfer (45) (2002) 3383–3396.
[2]    J.C. Han, Heat Transfer and Friction in Channels with Rib Roughened Walls, ASME Journal of Heat Transfer (106) (1984) 774–781.
[3]    R.L Webb, E.R.G. Eckert, Application of Rough Surface to Heat Exchanger Design, International Journal of Heat and Mass Transfer (15) (1972) 1647–1658.
[4]    R.L Webb, E.R.G. Eckert and R.J. Goldstein, Heat Transfer and Friction in Tubes With Repeated Rib Roughness, International Journal of Heat and Mass Transfer (14) (1971) 601–617.
[5]    N. Sheriff and P. Gumley, Heat Transfer and Friction Properties of surface with Discrete Roughness, International Journal of Heat and Mass Transfer (9) (1996) 1297–1320.
[6]    E.M. Sparrow and L.M. Hossfeld, Effect of Rounding of Protruding Edges on Heat transfer and Pressure Drop in a duct, International Journal of Heat and Mass Transfer (27) (1984) 1715–1723.
[7]    J.C. Han, L.R. Glicksman, and W.M. Rohsenow, An Investigation of Heat Transfer and Friction for Rib Roughed Surfaces, International Journal of Heat and Mass Transfer (21) (1978), 1142–1156.
[8]    D.L. Gee and R.L. Webb, Forced Convection Heat Transfer in Helically Rib Roughned Tubes, International Journal of Heat and Mass Transfer (23) (1980) 1127–1136.
[9]    M.J. Lewis, An Elementary analysis for Predicting the Momentum and Heat Transfer Characteristics of a Hydraulic Rough Surface, ASME Journal of Heat Transfer (97) (1975) 249-254.

[10]   R.P. Saini and Jitendra Verma, Heat transfer and friction factor correlations for a duct having dimple-shape artificial roughness for solar air heaters, Energy (33) (2008) 1277–1287

[11]   Santosh B. Bopche and Madhukar S. Tandale, Experimental investigations on heat transfer and frictional characteristics of a turbulator roughened solar air heater duct, International Journal of Heat and Mass Transfer (52) (2009) 2834–2848.

[12]   M.M. Sahu and J.L. Bhagoria, Augmentation of heat transfer coefficient by using 90o broken transverse ribs on absorber plate of solar air heater, Renewable Energy (30) (2005) 2057–2073.

[13]   M.K Mittal MK, Varun and R.P Saini, Singal SK. Effective efficiency of solar air heaters having different types of roughness elements on the absorber plate. Energy (32) (2007) 739–745.

[14]   Dhananjay Gupta, S.C Solanki and J.S Saini, Thermohydraulic performance of solar air heaters with roughened absorber plates, Solar Energy (61) (1997) 33–42.

[15]   Sukhmeet Singh, Subhash Chander and J.S. Saini, Exergy based analysis of solar air heater having discrete V-down rib roughness on absorber plate, Energy (37) (2012) 749–758.

[16]   Apurba Layek, J.S Saini and S.C Solanki. Second law optimization of a solar air heater having chamfered rib-groove roughness on absorber plate, Renewable Energy (32) (2007) 1967–1980.

[17]   M.K Gupta and S.C Kaushik, Performance evaluation of solar air heater for various artificial roughness geometries based on energy, effective and exergy efficiencies, Renewable Energy (34) (2009) 465–76.

[18]   Atul Lanjewar, J.L Bhagoria and R.M Sarviya, Heat transfer and friction in solar air heater duct with W-shaped rib roughness on absorber plate, Energy 36 (2011) 4531–4541.

[19]   A.R Jaurker, J.S Saini and B.K Gandhi, Heat transfer and friction characteristics of rectangular solar air heater duct using rig-grooved artificial roughness. Solar Energy (80) (2006) 895–907.

[20]   ASHRAE Standard 93–97, Methods of testing to determine the thermal performance of solar collectors, 1997.

[21]   S.J. Kline, F.A. McClintock, Describing uncertainties in single sample experiments, J. Mech. Eng. 75 (1953) 3–8.

**Madhukeshwara N.** working as a Lecturer in the department of Mechanical Engineering at B.I.E.T, Davanagere, Karnataka, INDIA. He has total eight years of experience in teaching Mechanical and Thermal engineering subjects. He is working in the area of heat transfer and fluid flow. He has supervised 8 undergraduate projects. At present he is guiding 2 undergraduate and 4 postgraduate projects. He has published around 11 research papers in journal/conferences of national and international repute.
E-mail address: madhu_keshwara@yahoo.co.in

**E. S. Prakash** working as a Professor and Head of the department of Mechanical Engineering at University B.D.T. College of Engineering, Davanagere, Karnataka, INDIA. He received Ph. D degree from Kuvempu University, B.R. Project, Shankaraghatta, INDIA He is working in the area of heat transfer and fluid flow. He is also working in the area of non conventional energy sources. He has supervised 6 postgraduate projects and 25 undergraduate projects. He has published around 38 research papers in journal/conferences of national and international repute. He is actively involved and successfully completed many sponsored research and consultancy projects.
E-mail address: prof_esp_ubdt@yahoo.co.in